IEEE Access
Multidisciplinary | Rapid Review | Open Access Journal

Received July 18, 2019, accepted July 30, 2019, date of publication August 6, 2019, date of current version August 20, 2019.

Digital Object Identifier 10.1109/ACCESS.2019.2933141

Aggregation Frequency Response Modeling for Wind Power Plants With Primary Frequency Regulation Service

JIANFENG DAI, (Student Member, IEEE), YI TANG, (Senior Member, IEEE), QI WANG, (Member, IEEE), AND PING JIANG
School of Electrical Engineering, Southeast University, Nanjing 210096, China

Corresponding author: Qi Wang (wangqi@seu.edu.cn)

This work was supported by the Science and Technology Project of State Grid Company (Research on Generation Control System and Operation Control Strategy of Ultra-High Proportion New Energy Grid).

ABSTRACT High-penetration wind power access to grid requires wind turbine generator (WTG) to provide frequency regulation service. Consequently, the frequency dynamics of wind power plants (WPPs) integrated system are changing; thus, it is necessary to investigate the dynamic frequency response of WPPs. In this paper, an analytical approach for an aggregated frequency response model for WPPs with primary frequency regulation service is presented and validated. First, different operation region of WTGs is fully taken into account, and a low-order wind power frequency response (WPFR) model with combined frequency control is deduced based on small signal analysis theory, which has been given in the form of symbolic transfer function. Afterwards, a system identification (SI) analytical method is proposed to aggregate a multi-machine WPFR model with heterogeneous parameters into a single equivalent model, which is called an aggregated WPFR (AWPFR) model, and this aggregation method is validated by the mathematical proof. Finally, the accuracy and effectiveness of the AWPFR model is verified through comparisons of simulation results obtained from the multi-machine WPFR model, detailed wind power plant (WPP) model and individual WPFR models, and the impact of the WTG parameters on the system frequency characteristics is analyzed and discussed. Such an aggregation model can provide a convenient way to describe the dynamic frequency response of WPPs by avoiding the need for modeling complex transient processes while maintaining a satisfactory level of accuracy.

INDEX TERMS Wind power plants, primary frequency regulation, frequency response model, multi-machine, system identification, mathematical proof, aggregation model.

I. INTRODUCTION

Variable-speed wind turbine generators (VSWTGs) have been more popular recently because of their maximum power tracking operation and flexible auxiliary controls by using converters [1]. Since these wind turbine generators (WTGs) replace a large number of conventional synchronous generators, the total system inertia gradually decreases due to the decoupling of the mechanical rotor speed and system frequency. Therefore, these types of WTGs are virtually insensitive to system frequency fluctuations, which degrade the frequency stability of the power system and reduce the ability to remain stable following a system fault or disturbance [2]–[5].

The associate editor coordinating the review of this manuscript and approving it for publication was Weixing Li.

In particular, the ever-growing tendency towards using wind power has resulted in WTGs providing a system frequency regulation service in the revised grid codes. Accordingly, a large number of significant studies have focused on using the auxiliary controls of the WTG to provide the inertial response and primary frequency response to the grid, with the corresponding frequency control strategies including inertial simulation control and deloading control [6]–[10].

However, only a small number of studies have investigated frequency response modeling of wind power (WPFR), which facilitates a quick and quantitative study of the frequency response characteristics without simulating the complex electromechanical and electromagnetic structures of the WTG. Similar to the traditional frequency response model of synchronous generators [11]–[14], the most common method employed in the WPFR model is to solve the frequency

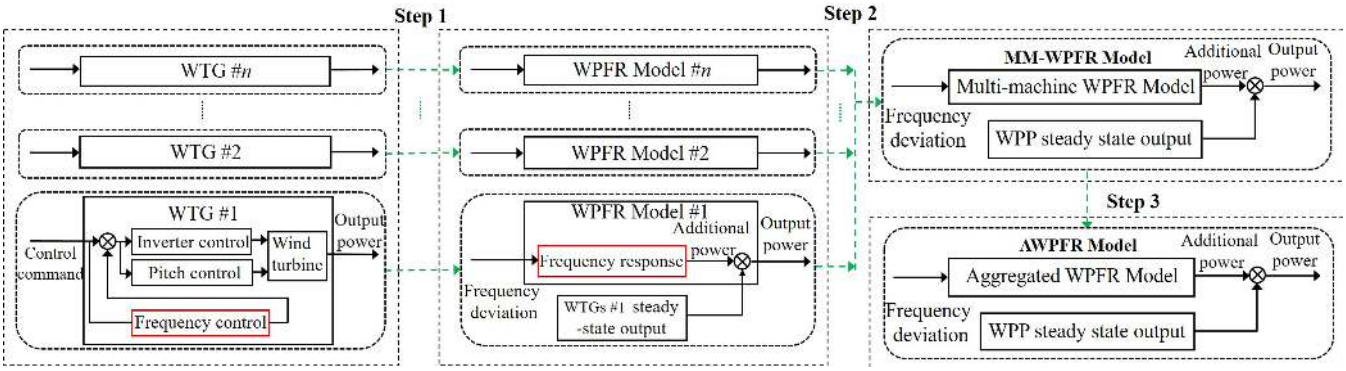

FIGURE 1. Process of developing the AWPFR model.

domain expression between the additional active variation and the frequency deviation. One method is to calculate the total inertia and damping of the system. An analytical model to evaluate the inertial and droop responses from a WPP for short-term frequency regulation was presented in [15]; however, only the available inertia and droop responses were expressed in equivalent numerical form, which did not consider the coupling characteristics of the frequency control loop and the internal parameters of the WTG and ignored the effects of the frequency control parameters. Thus, the model showed considerable error compared to the actual WPP. In addition, most of the remaining methods derive the equivalent frequency response model based on the state equation of the WTGs. A simplified linearized model of a controlled VSWTG for simulating the electromechanical dynamics in response to the network frequency deviations was proposed in [16], and a similar work was performed by the same author in [17]. Although works [16], [17] presented a low-order frequency response model of a WTG, only a pitch-angle-based deloading control strategy was taken into account, and the influence of the WTG parameters on the dynamic frequency response was not analyzed. Similarly, a nonlinear dynamic model using an input-to-state stability method was proposed to analyze the inertial frequency response of doubly fed induction-generator-based wind turbines in [18]; however, only the numerical form of the frequency response was given, and the corresponding transfer function form was not provided. Thus, it was unknown which WTG parameters define the frequency response model.

In general, as presented in the aforementioned studies, the different operation states of the WTG were not taken into account, and an individual frequency response model was assumed. It is not clear how to compute the equivalent response model parameters if the WPP consists of multiple WTGs with different operation states and heterogeneous control parameters. To fill the gaps in the present literature, this paper proposes a dynamic WPFR model that reflects the frequency dynamic response characteristics of WTGs under different operation states and heterogeneous control parameters and then aggregates the multi-machine WPFR (MM-WPFR) models into an aggregated

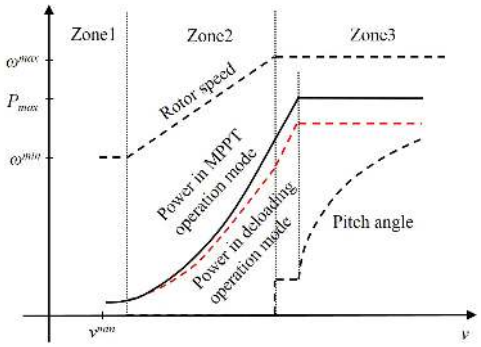

FIGURE 2. Operating curve of a WTG.

WPFR (AWPFR) model. Fig. 1 schematically illustrates the process of developing the AWPFR model.

The main contributions of this paper are as follows: 1) a low-order frequency response model of single wind power generation (WPFR) with combined frequency control considering different operation regions is deduced by using small signal analysis theory; 2) a system identification (SI) analytical method is proposed to aggregate the multi-machine WPFR models into a single equivalent AWPFR model; 3) a mathematical proof method is proposed to verify the effectiveness of the AWPFR model in mechanistic terms.

The organization of this paper is as follows. Section II deduces the single WPFR model. Section III presents the AWPFR model and proves it by mathematical proof. Section IV verifies the model by a comparative simulation, and the impact of different WTG parameters on frequency response is analyzed. Section V provides the conclusion.

II. SINGLE-WTG FREQUENCY RESPONSE MODEL

In this section, the frequency response model of a WTG is derived while respecting the different operating wind speed zones.

Wind turbines have different operation modes depending on the instantaneous input wind speed conditions, and these operating modes can generally be divided into three zones [19], [20], namely, the maximum power tracking zone, the constant speed zone and the constant power zone, as shown in Fig. 2. A frequency control strategy adapted

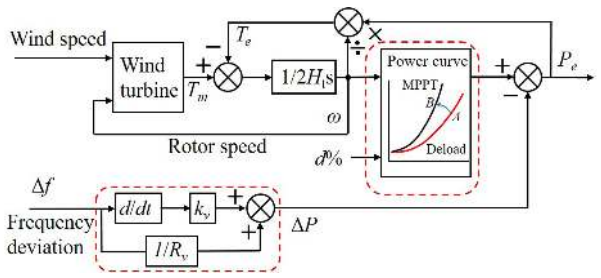

FIGURE 3. Combination of virtual inertia and over-speed deloading frequency control.

to different operation modes becomes important, and these modes will be elaborated in the following subsections.

A. ZONE I: OPERATION AT LOW WIND SPEEDS

In the low-wind-speed region, the available rotational kinetic energy provided by wind turbines is extremely low, and it is reasonable that the WTG will not participate in system frequency control in this region in this region in order to maintain the wind turbines in stable state as a priority, that because injecting additional active power into the grid will slow down the rotor speed of wind turbines, which may eventually lead to stalling of wind turbines [21]–[22]. Therefore, the WTG will not provide additional active power to the grid during frequency fluctuations, and the WPFR model is considered to be zero, namely, $G_{w\_l}(s) = 0$. And it should be emphasized that both the molecular and denominator coefficients of the $G_{w\_l}(s)$ are also zero. However, according to the statistics of WTG operation, few wind turbines operate in this region.

B. ZONE II: OPERATION AT MEDIUM WIND SPEEDS

In the medium-wind-speed region, with sufficient wind speed, the WTG will have enough reserve capacity to participate in frequency control. By referring to [23], [24], the dynamic frequency control strategy of a VSWTG based on combined virtual inertia control and overspeed-based deloading control is considered, as shown in Fig. 3. And the WTG output behavior can be described as:

$$P_m = \frac{\rho\pi r^2 v^3 C_p(\lambda, \beta = 0)}{2P_{base}} \tag{1}$$

$$P_{del} = (1-d)k_p\omega^3 \tag{2}$$

$$P_e = P_{del} + (P_{\max} - P_{del})\frac{\omega_{del} - \omega}{\omega_{del} - \omega_{\max}} \tag{3}$$

where P_m is the mechanical power, ρ is the air density, r is the blade length, v is the wind speed, C_p is the coefficient of the performance of the wind turbine, λ is the tip-speed ratio, β is the blade pitch angle, P_{base} is the rated power of the WTG, k_p is the scaling factor, P_e is the electrical power, P_{del} is the deloaded power, d is the deloading percentage, $P_{\max}$ is the maximum power, ω is the current rotor speed, and $\omega_{\max}$ and ω_{del} are the rotor speeds at $P_{\max}$ and P_{del}, respectively.

Here, we assume that all WTGs in this region are exposed to a constant wind speed pattern [25], the frequency response model of a WTG is analyzed using small signal analysis in this part [26]. The small signal state equation can be written as:

$$2H_t s\Delta\omega(s) = \Delta T_m(s) - \Delta T_e(s) \tag{4}$$

$$\Delta T_m(s) = \frac{\partial T_m}{\partial \omega}\Delta\omega(s) + \frac{\partial T_m}{\partial f}\Delta f(s) \tag{5}$$

$$\begin{aligned}\Delta T_e(s) = &-(\frac{1/R_v + k_v s}{\omega})\Delta f(s) \\ &+\left[2(1-d)k_p\omega + 2dk_p\omega\frac{(\omega_{del}-\omega)}{(\omega_{del}-\omega_{\max})}\right. \\ &\left.-\frac{k_p\omega^2}{(\omega_{del}-\omega_{\max})}\right]\Delta\omega(s)\end{aligned} \tag{6}$$

$$\Delta P_e(s) = \omega\Delta T_e(s) \tag{7}$$

where H_t is the inertia constant of the WTG, $\Delta\omega$ is the change in the rotor speed, ΔT_m and ΔT_e are the changes in the mechanical torque and electromagnetic torque, respectively, Δf is the change in the system frequency, and R_v and k_v are virtual inertia control parameters.

A low-order WPFR model can be derived and expressed in the form of small signal linearized transfer functions

$$G_{w\_m}(s) = \frac{\Delta P_e(s)}{\Delta f(s)} = -\frac{a_m s^2 + b_m s + c_m}{q_m s + 1} \tag{8}$$

where the q_m, a_m, b_m, $c_m$parameters are given in equation (9), as shown at the bottom of this page, k_C is the value of the partial derivative of C_p with respect to λ, and k_β is the value of the partial derivative of C_p with respect to β.

$$\begin{aligned}
q_m &= \frac{2H_t\omega^2}{2(1-d)k_p\omega^3 + k_p v^3 C_{\Pr ef} + 2dk_p\omega^3\frac{(\omega_{del}-\omega)}{(\omega_{del}-\omega_{\max})} - \frac{dk_p\omega^4}{(\omega_{del}-\omega_{\max})} - k_p k_C\omega v^2} \\
a_m &= \frac{2H_t\omega^2 k_v}{2(1-d)k_p\omega^3 + k_p v^3 C_{\Pr ef} + 2dk_p\omega^3\frac{(\omega_{del}-\omega)}{(\omega_{del}-\omega_{\max})} - \frac{dk_p\omega^4}{(\omega_{del}-\omega_{\max})} - k_p k_C\omega v^2} \\
b_m &= \frac{2H_t\omega^2/R_v + k_v k_p v^3 C_{\Pr ef} - (1-d)k_v k_p\omega^3 - dk_v k_p\omega^3\frac{(\omega_{del}-\omega)}{(\omega_{del}-\omega_{\max})} - k_v k_p k_C\omega v^2}{2(1-d)k_p\omega^3 + k_p v^3 C_{\Pr ef} + 2dk_p\omega^3\frac{(\omega_{del}-\omega)}{(\omega_{del}-\omega_{\max})} - \frac{dk_p\omega^4}{(\omega_{del}-\omega_{\max})} - k_p k_C\omega v^2} \\
c_m &= -\frac{\frac{k_p v^3 C_{\Pr ef}}{R_v} - \frac{(1-d)k_p\omega^3}{R_v} - \frac{k_p k_C\omega v^2}{R_v} - \frac{dk_p\omega^3(\omega_{del}-\omega)}{R_v(\omega_{del}-\omega_{\max})}}{2(1-d)k_p\omega^3 + k_p v^3 C_{\Pr ef} + 2dk_p\omega^3\frac{(\omega_{del}-\omega)}{(\omega_{del}-\omega_{\max})} - \frac{dk_p\omega^4}{(\omega_{del}-\omega_{\max})} - k_p k_C\omega v^2}
\end{aligned} \tag{9}$$

C. ZONE III: OPERATION AT LOW WIND SPEEDS

In the medium-wind-speed region, the rotor speed of a wind turbine reaches the maximum limit. It is no longer possible to achieve the deloading operation through over-speed control. By referring to [16], [17], the dynamic frequency control strategy of a VSWTG based on combined virtual inertia control and pitch-angle-based deloading control is considered, as shown in Fig. 4.

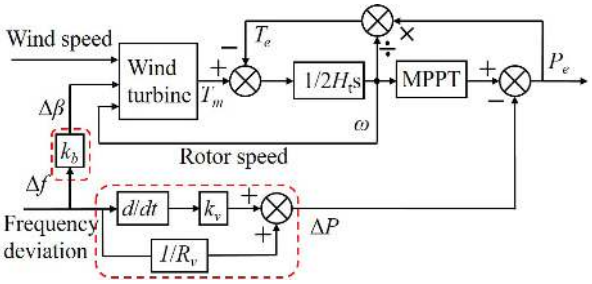

FIGURE 4. Combination of virtual inertia and pitch angle frequency control.

Similar to the expressions for the generator power (1) -(3) in zone II, the WTG output behavior can be described as

$$P_m = \frac{\rho\pi r^2 v^3 C_p(\lambda, \beta = \beta_0)}{2P_{base}} \tag{10}$$

$$P_e = k_p \omega_{\max}^3 \tag{11}$$

where β_0 is the pitch angle of the wind turbine for the deloading operation.

New options introduced by the pitch angle controller can be described as

$$\Delta\beta = k_b \Delta f \tag{12}$$

where $\Delta\beta$ is the change in the blade pitch angle and k_b is the proportionality coefficient of pitch-based frequency control method.

The corresponding small signal state equation can be written as:

$$\Delta T_m(s) = \frac{\partial T_m}{\partial \omega}\Delta\omega(s) + \frac{\partial T_m}{\partial C_p}\left(\frac{\partial C_p}{\partial \lambda}\Delta\lambda(s) + \frac{\partial C_p}{\partial \beta}\frac{\partial \beta}{\partial f}\Delta f(s)\right) \tag{13}$$

$$\Delta T_e(s) = -\left(\frac{1/R_v + k_v s}{\omega}\right)\Delta f(s) + 2k_p\omega\Delta\omega(s) \tag{14}$$

where $\Delta\lambda$ is the change in the tip-speed ratio.

The low-order WPFR model in this region can be derived and expressed in the form of small signal linearized transfer functions as follows:

$$G_{w\_h}(s) = \frac{\Delta P_e(s)}{\Delta f(s)} = -\frac{a_h s^2 + b_h s + c_h}{q_h s + 1} \tag{15}$$

where

$$q_h = \frac{2H_t\omega^2}{2k_p\omega^3 + k_p v^3 C_{\Pr ef} - k_p k_C \omega v^2}$$

$$a_h = \frac{2H_t\omega^2 k_v}{2k_p\omega^3 + k_p v^3 C_{\Pr ef} - k_p k_C \omega v^2}$$

$$b_h = \frac{2H_t\omega^2 \frac{1}{R_v} - 3k_v k_p \omega^2 + k_v(2k_p\omega^3 + k_p v^3 C_{\Pr ef} - k_p k_C \omega v^2)}{2k_p\omega^3 + k_p v^3 C_{\Pr ef} - k_p k_C \omega v^2}$$

$$c_h = \frac{\frac{1}{R_v}(2k_p\omega^3 + k_p v^3 C_{\Pr ef} - k_p k_C \omega v^2) - 3\omega^2\left(\frac{1}{R_v} + k_p k_\beta k_b v^2\right)}{2k_p\omega^3 + k_p v^3 C_{\Pr ef} - k_p k_C \omega v^2} \tag{16}$$

By comparing transfer function (8) and transfer function (15), it can be seen that the transfer function order of the WPFR model in the middle-wind-speed zone and high-wind-speed zone are the same, and the difference is only the molecular and denominator coefficients. Thus, the unified form of the low-order WPFR model under full wind conditions can be written as

$$G_w(s) = \frac{\Delta P_e(s)}{\Delta f(s)} = -\frac{as^2 + bs + c}{qs + 1} \tag{17}$$

Therefore, the frequency dynamic response characteristics of the WTG can be analyzed by (17) instead of performing a time-domain simulation. However, it should be noted that the values of q, a, b, and c are related not only to the wind speed region as mentioned in the above analysis but also to the operation parameters and control parameters of the WTG. If the actual system consists of multiple wind turbines with heterogeneous parameters, we need to calculate the equivalent WPFR model parameters, namely, the premise behind using equation (17) is that multiple WTGs with heterogeneous parameters in a specific wind speed region can be aggregated into an equivalent WTG.

III. ANALYTICAL METHOD FOR THE AGGREGATE MODEL

Based on the analysis in Section II, this section demonstrates how to aggregate the MM-WPFR model into the AWPFR model.

A. FORMULATION OF THE AWPFR MODEL

Assume that the WPP has several wind turbines with heterogeneous parameters, and all of them participate in the frequency control of the grid. The aggregation of the WPP frequency response model is shown in Fig. 5.

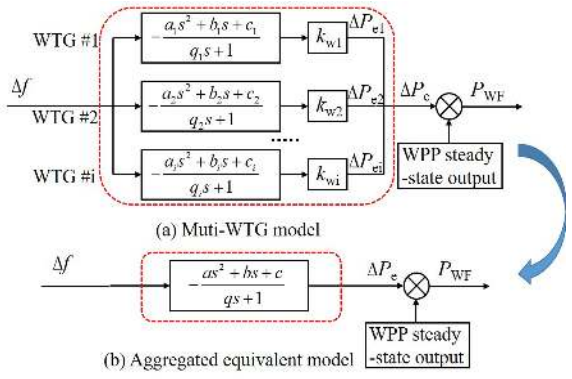

FIGURE 5. Aggregation of the wind power frequency response model.

As seen from the dashed box in Fig. 5, the transfer function of a single WTG can represent that of multiple WTGs.

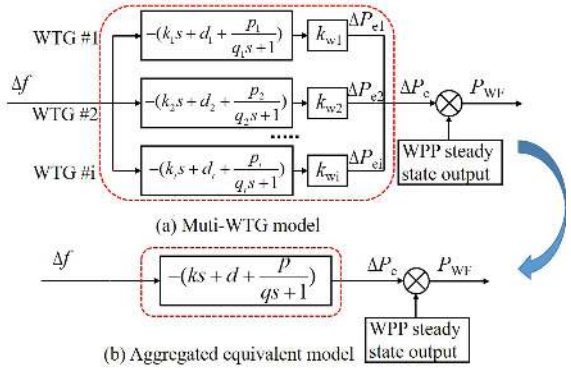

FIGURE 6. New manifestation of aggregated frequency response model.

Thus, (18) can be obtained:

$$\sum_{i=1}^{N} k_{wi} \frac{a_i s^2 + b_i s + c_i}{q_i s + 1} = \frac{as^2 + bs + c}{qs + 1} \tag{18}$$

where k_{wi} represents the portion of the rated power of WTG#*i* with respect to the WPP, q_{i}, a_{i}, b_{i}, and c_{i} are the transfer function parameters of the frequency response model of WTG#*i*.

To simplify the analysis, the transfer function of (18) is split into two parts as follows:

$$\frac{as^2 + bs + c}{qs + 1} = (ks + d) + \frac{p}{qs + 1} \tag{19}$$

where

$$k = \frac{a}{q}, \quad d = \frac{bq - a}{q^2}, \quad p = c - d \tag{20}$$

Therefore, another manifestation of the Fig. 5 can be written as:

Then, equation (18) can be expressed as:

$$\sum_{i=1}^{N} k_{wi} \left(k_i s + d_i + \frac{p_i}{q_i s + 1} \right) = \left(ks + d + \frac{p}{qs + 1} \right) \tag{21}$$

Traditionally, the parameters $X = \{k, d, p, q\}$ can be obtained by SI [27]–[29]. The basic principle is to find the optimal X, and the goal is obtaining an equivalent single WTG output that is as close as possible to the output of multiple WTGs. Therefore, this paper proposes an analytical method to calculate X. It can be seen that a larger weighting factor means that WTG#*i* has a greater impact on X. Thus, it can reasonably guess that the parameters of the AWPFR model are equal to the weighted average of those of each WTG. We define the weighted average coefficient as λ_{i}; then, we have the following formula:

$$X = \sum_{i=1}^{N} \lambda_i X_i \tag{22}$$

The following section will demonstrate that the parameters of the AWPFR model can be obtained with high precision by equation (22). Since equation (21) has been split into two parts, we only need to prove that the two equations of (21) are valid

$$\sum_{i=1}^{N} k_{wi} (k_i s + d_i) = ks + d \tag{23}$$

$$\sum_{i=1}^{N} k_{wi} \frac{p_i}{q_i s + 1} = \frac{p}{qs + 1} \tag{24}$$

By analyzing the structures of equations (23) and (24), it can be found that the equivalence of the parameters k, d, and p is associated with the weighted average coefficient k_{w}. Therefore, the parameters of k, d, and p can be directly obtained by (23) and (24), and $\lambda_{\mathrm{i}} = k_{\mathrm{mi}}$. The corresponding results are as follows:

$$\begin{aligned} k &= \sum_{i=1}^{N} k_{wi} k_i \\ d &= \sum_{i=1}^{N} k_{wi} d_i \\ p &= \sum_{i=1}^{N} k_{wi} p_i \end{aligned} \tag{25}$$

The equivalence of the parameter q is the most complex one, which is simultaneously associated with k_{w} and p. In equation (24), the effect of p_{i} can be seen as a virtual droop coefficient generated by combined frequency control; thus, the value of p_{i} is correlated to the rated power of the WTG, the weighted average coefficient of which is only determined by k_{mi}. Therefore, a proof of an equivalent q value is the focus of this paper.

Based on the above analysis, the equivalent value of p_{i} is given by:

$$p = \sum_{i=1}^{N} k_{wi} p_i = \sum_{i=1}^{N} \alpha_i \tag{26}$$

where α_{i} is the equivalent gain.

To simplify the description, we define the normalized gain γ_{i} of each portion in equation (24).

$$\gamma_i = \alpha_i / \sum_{i=1}^{N} \alpha_i \tag{27}$$

$$\sum_{i=1}^{N} \gamma_i = 1 \tag{28}$$

Therefore, the parameters of $q$can be obtained by (22) and $\lambda_{\mathrm{i}} = \gamma_{\mathrm{i}}$, and we only need to prove that the following equation is valid.

$$\sum_{i=1}^{N} \gamma_i \frac{1}{q_i s + 1} = \frac{1}{qs + 1} \tag{29}$$

B. MATHEMATICAL VALIDATION

In this part, equation (29) is proved by mathematical proof. The following steps first take two WTGs as an example and then extend it to multi-WTG systems.

1) TWO-WTG CASE

The first step is to consider a simple example that contains only two WTGs, namely, $N = 2$. What needs to be proved here is that the magnitude of the error function $e_w(s)$ is negligible, where $e_w(s)$ is defined as:

$$e_w(s) = \gamma_1 \frac{1}{q_1 s + 1} + \gamma_2 \frac{1}{q_2 s + 1} - \frac{1}{qs + 1} = \frac{P_w(s)}{Q_w(s)} \tag{30}$$

where

$$\frac{P_w(s)}{Q_w(s)} = \frac{m_2 s^2 + m_1 s + m_0}{n_3 s^3 + n_2 s^2 + n_1 s + n_0} \tag{31}$$

First, we analyze the frequency characteristics of the error function $e_w(s)$. Based on (30) and (31), we can deduce the coefficients of $P_w(s)$ as follows:

$$\begin{aligned} m_0 &= \gamma_1 + \gamma_2 - 1 \\ m_1 &= (\gamma_1 + \gamma_2 - 1)(q_1 + q_2) \\ m_2 &= \gamma_1 \gamma_2 (q_1 - q_2)^2 \end{aligned} \tag{32}$$

Thus, the expression of $m_0 = m_1 = 0$, and the nonzero term is m_2. Obviously, it indicates that $|m_2|$ is proportional to the square of $|q_1\text{-}q_2|$.

since

$$\gamma_1 \gamma_2 \le (\frac{\gamma_1 + \gamma_2}{2})^2 = 0.25 \tag{33}$$

The upper bound of $|m_2|$ can be written as

$$\begin{aligned} |m_2| &= \left| \gamma_1 \gamma_2 (q_1 - q_2)^2 \right| \\ &\le 0.25 \left| (q_1 - q_2)^2 \right| \end{aligned} \tag{34}$$

Similarly, we also deduce the coefficients of $Q_w(s)$ as follows

$$\begin{aligned} n_0 &= 1 \\ n_1 &= q_1 + q_2 + q \\ n_2 &= q(q_1 + q_2) + q_1 + q_2 \\ n_3 &= q q_1 q_2 \end{aligned} \tag{35}$$

It can be seen from (32) and (35) that m_2 is more sensitive to $|q_1\text{-}q_2|$ than n_2. Thus, in the worst case, the ratio $|m_2/n_2|$ is maximized when $\gamma_1 = \gamma_2$, and $|q_1\text{-}q_2|$ reaches its maximum. For example, for $q_1 = 5.8758$ and $q_2 = 4.3036$, the upper bound of $|m_2/n_2|$ is:

$$\left| \frac{m_2}{n_2} \right| \le \frac{0.25(q_1 - q_2)^2}{q_1 q_2 + q(q_1 + q_2)} < 0.00804 \tag{36}$$

Combining (31) and (36), it can be seen that the magnitude of $e_w(s)$ is much smaller than 1. In addition, to represent the error of ΔP_m more profoundly, we define the per-unit error function $e_{w.pu}(s)$ as follows:

$$e_{w.pu}(s) = \frac{e_w(s)}{\Delta P_w(s)} = \frac{e_w(s)}{\gamma_1 \frac{1}{q_1 s + 1} + \gamma_2 \frac{1}{q_2 s + 1}} \tag{37}$$

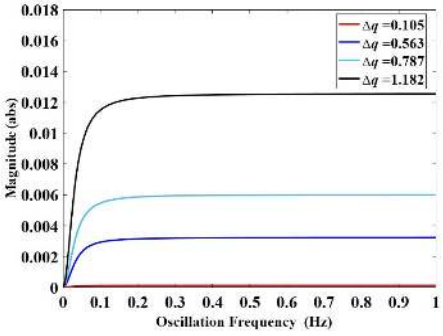

FIGURE 7. Frequency characteristics of $e_{w.pu}(s)$.

The frequency characteristics of $e_{w.pu}(s)$ under various Δq is presented in Fig. 7. The magnitude of $e_{w.pu}(s)$ is less than 0.012, which is negligible and will significantly decrease if Δq decreases. Therefore, the case of (29) is proven, that is, it is further explained that (24) and (22) are also proven.

2) MULTI-WTG CASE

Next, the multi-WTG case is proven. The idea of multi-WTG aggregation is to merge the WTGs one by one. Since the parameters k, d, and p can be obtained directly by the weighted average coefficient k_m as shown in (25), only the equivalent process of parameter q needs to be proved here, as shown in Fig. 8.

Assume that a WPP consists of N WTGs, and all wind turbines with the same parameters are classified into one category, and former k WTG groups can be aggregated into a single WTG:

$$q_{\Sigma k} = \sum_{i=1}^{k} \gamma_i q_i = \sum_{i=1}^{k} \frac{\alpha_i}{\alpha_{\Sigma k}} q_i \tag{38}$$

Then, we need to prove that the $(k+1)$-th WTG group can also be combined with this equivalent WTG.

$$q_{\Sigma(k+1)} = \sum_{i=1}^{k+1} \gamma_i q_i = \sum_{i=1}^{k} \frac{\alpha_i}{\alpha_{\Sigma(k+1)}} q_i \tag{39}$$

Assuming that the former merged k WTGs are regarded as the k-th equivalent WTG, and it was considered as the k-subsystem of the whole WPP, the base power of the defined subsystem can be written as

$$\alpha_{\Sigma k} = \sum_{i=1}^{k} \alpha_i \tag{40}$$

If the former k-subsystem and the $(k+1)$-th WTG group are merged, the merged $k+1$ subsystem consists of these two parts, as shown in Fig. 8, where $S_{\Sigma k}$ and S_{k+1} are the rated capacity of the former k-subsystem and the $(k+1)$-th WTG group respectively.

Then, the base power of the new merged $k+1$ subsystem is reconfigured, and the normalized gain of the former k-subsystem and the $(k+1)$-th WTG group can be

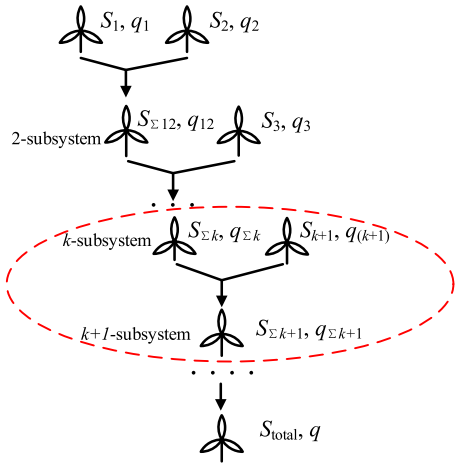

FIGURE 8. Aggregation of the wind power frequency response model.

expressed as

$$\gamma_{\Sigma k} = \frac{\alpha_{\Sigma k}}{\alpha_{\Sigma(k+1)}} = \frac{\alpha_{\Sigma k}}{\alpha_{\Sigma k} + \alpha_{k+1}}$$
$$\gamma_{k+1} = \frac{\alpha_{k+1}}{\alpha_{\Sigma(k+1)}} = \frac{\alpha_{k+1}}{\alpha_{\Sigma k} + \alpha_{k+1}} \tag{41}$$

Then, the equivalent parameter q of the (k + 1)-subsystem can be derived as follows:

$$\begin{aligned} q_{\Sigma(k+1)} &= \gamma_{\Sigma k} q_{\Sigma k} + \gamma_{k+1} q_{(k+1)} \\ &= \frac{\alpha_{\Sigma k}}{\alpha_{\Sigma k} + \alpha_{k+1}} \sum_{i=1}^{k} \gamma_i q_i + \frac{\alpha_{k+1}}{\alpha_{\Sigma k} + \alpha_{k+1}} q_{(k+1)} \\ &= \frac{\alpha_{\Sigma k}}{\alpha_{\Sigma k} + \alpha_{k+1}} \sum_{i=1}^{k} (\frac{\alpha_i}{\alpha_{\Sigma k}} q_i) + \frac{\alpha_{k+1}}{\alpha_{\Sigma k} + \alpha_{k+1}} q_{(k+1)} \\ &= \sum_{i=1}^{k} (\frac{\alpha_i}{\alpha_{\Sigma k} + \alpha_{k+1}} q_i) + \frac{\alpha_{k+1}}{\alpha_{\Sigma k} + \alpha_{k+1}} q_{(k+1)} \\ &= \sum_{i=1}^{k+1} (\frac{\alpha_i}{\alpha_{\Sigma(k+1)}} q_i) \\ &= \sum_{i=1}^{k+1} \gamma_i q_i \end{aligned} \tag{42}$$

Similar to the above steps, the parameters q_i of the N wind turbines can be combined into one equivalent value. In addition, combined with the equivalent result of the parameters k, d, and p, all WTGs can be equivalent to one WTG. Thus, (22) can be proved for any N value because it can satisfy equations (21) and (18) with higher precision.

It is inevitable that a certain error will be introduced in each merger. However, after multiple merges, the former equivalent gain $\gamma_{\Sigma k}$ is much larger than γ_{k+1}, namely, $\gamma_{\Sigma k} >> \gamma_{k+1}$. It can be seen from (32) that the value of m_2 will be extremely small, and $q_{(k+1)}$ will not have large fluctuations during each merger. Therefore, the cumulative error after multiple mergers will gradually converge, and it will also be within the permitted scope. The next section will evaluate whether the error is significant by simulation and comparison.

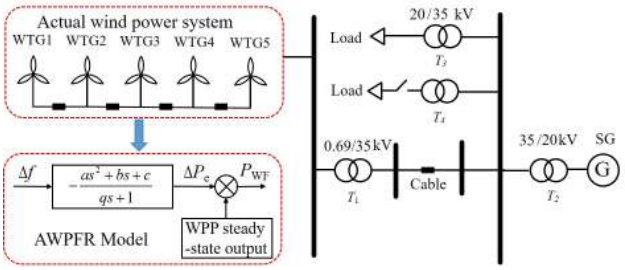

FIGURE 9. Simulation system.

TABLE 1. Parameters of the 5-WTG WPFR model.

WTG.No.	k	d	p	q	k_w	γ
1	0.1	19.9757	13.8407	5.2487	0.2	0.084
2	0.15	22.1896	23.7950	5.4726	0.16	0.115
3	0.2	24.9513	33.888	4.6856	0.24	0.245
4	0.25	28.5258	43.4573	5.8677	0.267	0.35
5	0.3	33.2687	51.3374	4.7906	0.133	0.206
Equ.	0.199	25.57	33.139	5.2059	1	1

IV. CASE STUDY

In this section, the performance of the developed AWPFR model is verified against the MM-WPFR model, the detailed WPP model, and individual WPFR models; then, the impact of WTG parameters on dynamic frequency response is analyzed.

A. MODELING VERIFICATION

The test system consists of a Synchronous Generators (SG) of 36 MWA, a static load of 30 MW and an 8.5 MW WPP consists of 3 1.5-MW PMSGs and 2 2-MW PMSGs. The test system is built in the PSCAD/EMTDC simulation environment. As shown in Fig. 9, the entire simulation duration is 20 s. We apply a sudden increase in the load, initiated at 2 s. The SG and WTG parameters are listed in Appendix.

1) AWPFR MODEL VS. THE MM-WPFR MODEL

Since the model parameters in X can be any value within the normal stable range, we should simulate the worst case that maximizes the frequency deviation. Therefore, this paper sets the parameter X of the different WTGs according to a growth distribution; this distribution is the worst case because $X = \{k, d, p, q\}$ deviate more from the average values and in a wider range. According to (9), (16) and (20), the equivalent parameters $X = \{k, d, p, q\}$ of each WTG can be calculated by setting the WTG parameters such as k_v, R_v, k_b, and H_t, respectively. The detailed parameters of the WTGs are presented in Appendix A, and the model parameters X are listed in Table 1.

Fig. 10 compares the frequency and additional power responses and the corresponding response error of the proposed AWPFR model and the MM-WPFR model. Note that the additional power of the MM-WPFR model is the sum

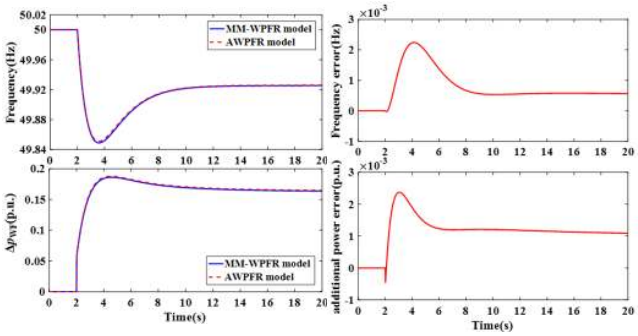

FIGURE 10. Comparison of the AWPFR model with the MM-WPFR model.

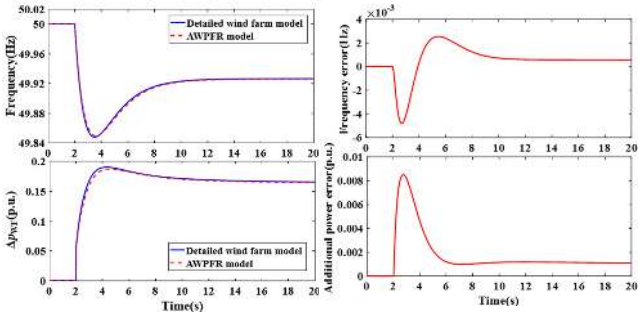

FIGURE 11. Comparison of the AWPFR model with the detailed WPP model.

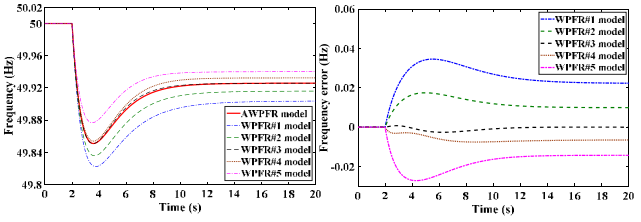

FIGURE 12. Comparison of the AWPFR model with individual WPFR models.

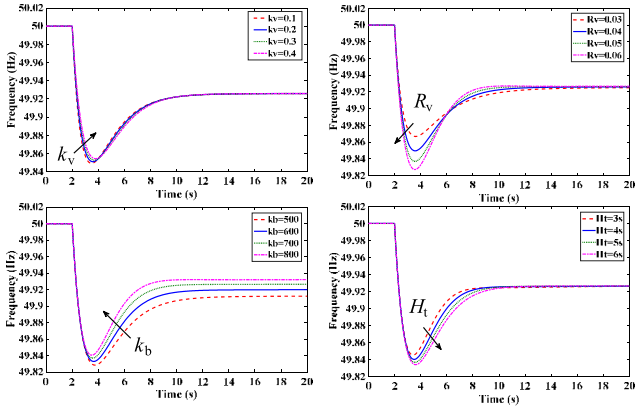

FIGURE 13. Impacts of different parameters on the AWPFR models.

of 5 WTGs. It can be seen that there is not much difference between the frequency and additional power response curves obtained from the two models, and the errors in the frequency and additional power responses are both less than 0.0024 in the worst case, which means that the AWPFR model can replace the MM-WPFR model with high accuracy.

2) AWPFR MODEL V.S. A DETAILED WPP MODEL

The AWPFR model is compared with an actual WPP system in terms of frequency and additional power responses and the corresponding error, as shown in Fig. 11.

The frequency and additional power response curves obtained from the AWPFR model and detailed WPP model are quite close. The maximum errors in the frequency and additional power are 0.0049 Hz and 0.0082 pu, respectively. In addition, the computation time of the AWPFR model is 5 s, while that of the detailed actual model is 119 s. Therefore, the established AWPFR model has a good accuracy and simulation time advantages.

3) AWPFR MODEL VS. INDIVIDUAL WPFR MODELS

The AWPFR model is compared with five WPFR models, which are named WPFR#1, WPFR#2, WPFR#3, WPFR#4 and WPFR#5, and the WPFR model parameters for each are listed in TABLE 1. The corresponding description of the WPFR#1 model is that five WTGs have the same parameters as WTG1, and the descriptions of WPFR#2, WPFR#3, WPFR#4 and WPFR#5 are similarly known.

A comparison of the AWPFR model with five WPFR models in terms of frequency response is shown in Fig. 12. It can be seen that if only the individual WFPR model is assumed to analyze the frequency dynamics of the whole WPP, there is a large difference between the frequency response curves from the AWPFR model (closer to the actual detailed wind farm model, as shown in Fig. 11) and the five WPFR models, especially when the WTG parameters vary greatly; the error in the frequency response is as high as 0.039 Hz in the WPFR#5 case, which means that the individual WPFR model would have large frequency dynamic performance deviations when the WTGs work in quite different operation states with different control parameters. Thus, it is unreasonable to employ the individual WPFR model to analyze the frequency dynamics of a WPP, and the necessity of the AWPFR model in this paper has been proven.

B. IMPACTS OF THE WTG PARAMETERS ON THE AWPFR MODEL

The description in Section II and Section III suggests that the dynamic frequency performances of the WPP integrated system are restrained by the WTG properties, which are determined by the control parameters and the initial operating states. A detailed simulation test to obtain the influence of k_v, R_v, k_b, and H_t on the AWPFR model is carried out, as shown in Fig. 13.

The impact of parameter k_v from virtual-inertia-based frequency control on the AWPFR shows that an increase in k_v causes the rate of change of the frequency (ROCOF) to gradually decrease and the frequency nadir to slightly increase, while the steady-state frequency is not affected. Additionally, the impact of the droop gain R_v from virtual-inertia-based

frequency control on the AWPFR shows that an increase in R_v causes the frequency nadir to gradually decrease, and the droop gain has no significant effect on the steady-state frequency. This demonstrates that virtual-inertial-based frequency control of WTGs can contribute to the frequency stabilization, and a larger k_v and smaller R_v can promote more transient rotational kinetic energy released by the WTGs, resulting in playing a greater role. Nevertheless, setting a higher k_v and a smaller R_v may result in a second drop in the network frequency, which is not conducive to system frequency security.

The impact of parameter k_b from pitch-angle-based frequency control on the AWPFR shows that k_b does not have any effect on the ROCOF but has a significant impact on the frequency nadir and the steady-state frequency values. An increase in k_b produces an increased frequency nadir and steady-state frequency values. This means that the frequency nadir and the steady-state frequency values are sensitive to a change in parameter k_b. The main reason is that a higher k_b value will result in a larger reserve power controlled by pitch-control-based deloading control.

Finally, the impact of different WTG inertia constants H_t on the AWPFR model shows that the WTG inertia constant H_t also has a significant impact on the AWPFR. An increase in H_t produces an increased frequency nadir, while the ROCOF and steady-state frequency are not affected by varying H_t. This is mainly because the heavier WTGs (larger H_t) will have a slower frequency response. This is precisely the reason why the AWPFR characteristics are affected by the initial operating state parameters of the WTGs.

V. CONCLUSION

In this study, an aggregated frequency response model for WPPs with primary frequency regulation service is developed and validated. A single linearized WPFR model considering different WTG operation regions is first presented by using small signal analysis principle. Then, a SI analytical method is proposed to obtain the AWPFR model parameters based on the multi-machine WPFR model parameters.

(1) The WPFR model takes into account different operating regions dependent on the instantaneous input wind speed and is expressed as a cover transfer function between the additional power variation Δp_e and the frequency deviation Δf of the WTG with combined frequency control, which clearly shows the key parameters affecting the frequency response and gives a more intuitive description of the frequency dynamic behavior.

(2) A SI analytical method is proposed to aggregate the MM-WPFR model with high accuracy, as proven by mathematical proof and a simulation verification. In addition, the AWPFR model can accurately replace the frequency response of detailed WPPs. Therefore, the proposed AWPFR model can provide a simpler, clearer and faster way of evaluating the dynamic frequency response characteristic of WPPs without simulating the complex electromechanical and electromagnetic structures of the WTGs.

(3) The impact of the WTG parameters on the frequency response is investigated and discussed. The impact of the primary frequency control parameters (e.g., k_v, R_v and k_b) and initial operating states parameter (e.g., H_t) are significant due to the coupling effect of the power electronics interface caused by the auxiliary frequency controller. Similarly, these key parameters also have a great impact on the aggregation of the WPFR models, which determine the equivalent parameters (e.g., k, d, p, q) of the WPFR model.

APPENDIX

SG Parameters: Rated power 36 MW, $X_d = 0.361$, $X_d' = 0.1502$, $X_d'' = 0.1$, $X_q = 0.2386$, $X_q'' = 0.2$, $R_s = 0.03$, $X_l = 0.0826$, $T_{d0}' = 8.96$, $T_{d0}'' = 0.05$, $T_{q0}'' = 0.03$, $H = 5$s, $D = 1$, $R = 0.05$, $F_H = 0.3$, $T_R = 7$s, $T_c = 0.2$s, $T_G = 0.3$.

WTG1 Parameters: Rated power 1.5 MW, $H_t = 4.5$, $\omega_0 = 0.8054$, $v_0 = 0.875$, $k_p = 0.73$, $C_{pref} = 0.9029$, $\lambda_{ref} = 0.96648$, $k_{cp} = 0.0771$, $k_\beta = -0.1014$, $k_v = 0.1$, $R_v = 0.05$, $k_b = 600$.

WTG2 Parameters: Rated power 1.5 MW, $H_t = 5.04$, $\omega_0 = 0.8763$, $v_0 = 0.896$, $k_p = 0.73$, $C_{pref} = 0.9029$, $\lambda_{ref} = 0.96648$, $k_{cp} = 0.0821$, $k_\beta = -0.1108$, $k_v = 0.15$, $R_v = 0.045$, $k_b = 650$.

WTG3 Parameters: Rated power 1.5 MW, $H_t = 4.5$, $\omega_0 = 0.9268$, $v_0 = 0.935$, $k_p = 0.73$, $C_{pref} = 0.9029$, $\lambda_{ref} = 0.96648$, $k_{cp} = 0.0865$, $k_\beta = -0.1224$, $k_v = 0.2$, $R_v = 0.004$, $k_b = 700$.

WTG4 Parameters: Rated power 2 MW, $H_t = 6$, $\omega_0 = 0.9964$, $v_0 = 0.982$, $k_p = 0.73$, $C_{pref} = 0.94$, $\lambda_{ref} = 1.12$, $k_{cp} = 0.0908$, $k_\beta = -0.1309$, $k_v = 0.25$, $R_v = 0.035$, $k_b = 750$.

WTG5 Parameters: Rated power 2 MW, $H_t = 5.08$, $\omega_0 = 1.1174$, $v_0 = 1$, $k_p = 0.73$, $C_{pref} = 0.94$, $\lambda_{ref} = 1.12$, $k_{cp} = 0.0921$, $k_\beta = -0.1421$, $k_v = 0.3$, $R_v = 0.003$, $k_b = 800$.

REFERENCES

[1] F. Blaabjerg, M. Liserre, and K. Ma, "Power electronics converters for wind turbine systems," *IEEE Trans. Ind. Appl.*, vol. 48, no. 2, pp. 708–719, Apr. 2012.

[2] H. Gu, R. Yan, and T. K. Saha, "Minimum synchronous inertia requirement of renewable power systems," *IEEE Trans. Power Syst.*, vol. 33, no. 2, pp. 1533–1543, Mar. 2018.

[3] N. Nguyen and J. Mitra, "An analysis of the effects and dependency of wind power penetration on system frequency regulation," *IEEE Trans. Sustain. Energy*, vol. 7, no. 1, pp. 354–363, Jan. 2016.

[4] A. B. T. Attya and J. L. Dominguez-García, "Insights on the provision of frequency support by wind power and the impact on energy systems," *IEEE Trans. Sustain. Energy*, vol. 9, no. 2, pp. 719–728, Apr. 2018.

[5] P. K. Naik, N.-K. C. Nair, and A. K. Swain, "Impact of reduced inertia on transient stability of networks with asynchronous generation," *Int. Trans. Elect. Energy Syst.*, vol. 26, no. 1, pp. 175–191, Jan. 2016.

[6] X. Yingcheng and T. Nengling, "Review of contribution to frequency control through variable speed wind turbine," *Renew. Energy*, vol. 36, no. 6, pp. 1671–1677, 2011.

[7] Z. Wu, W. Gao, T. Gao, W. Yan, H. Zhang, S. Yan, and X. Wang, "State-of-the-art review on frequency response of wind power plants in power systems," *J. Mod. Power Syst. Clean Energy*, vol. 6, no. 1, pp. 1–16, Jan. 2018.
[8] M. E. Lotfy, T. Senjyu, M. A. Farahat, A. F. Abdel-Gawad, and A. Yona, "Enhancement of a small power system performance using multi-objective optimization," *IEEE Access*, vol. 5, pp. 6212–6224, Apr. 2017.
[9] G. Magdy, G. Shabib, A. A. Elbaset, and Y. Mitani, "Optimized coordinated control of LFC and SMES to enhance frequency stability of a real multi-source power system considering high renewable energy penetration," *Protection Control Mod. Power Syst.*, vol. 3, no. 1, Dec. 2018, Art. no. 39.
[10] X. Zhang, X. Zha, S. Yue, and Y. Chen, "A frequency regulation strategy for wind power based on limited over-speed de-loading curve partitioning," *IEEE Access*, vol. 6, pp. 22938–22951, 2018.
[11] P. M. Anderson and M. Mirheydar, "A low-order system frequency response model," *IEEE Trans. Power Syst.*, vol. 5, no. 3, pp. 720–729, Aug. 1990.
[12] D. L. H. Aik, "A general-order system frequency response model incorporating load shedding: Analytic modeling and applications," *IEEE Trans. Power Syst.*, vol. 21, no. 2, pp. 709–717, May 2006.
[13] S. Liao, J. Xu, Y. Sun, W. Gao, X.-Y. Ma, M. Zhou, Y. Qu, X. Li, J. Gu, and J. Dong, "Load-damping characteristic control method in an isolated power system with industrial voltage-sensitive load," *IEEE Trans. Power Syst.*, vol. 31, no. 2, pp. 1118–1128, Mar. 2016.
[14] H. Pulgar-Painemal, Y. Wang, and H. Silva-Saravia, "On inertia distribution, inter-area oscillations and location of electronically-interfaced resources," *IEEE Trans. Power Syst.*, vol. 33, no. 1, pp. 995–1003, Jan. 2018.
[15] H. Ye, W. Pei, and Z. Qi, "Analytical modeling of inertial and droop responses from a wind farm for short-term frequency regulation in power systems," *IEEE Trans. Power Syst.*, vol. 31, no. 5, pp. 3414–3423, Sep. 2016.
[16] S. Ghosh and N. Senroy, "Electromechanical dynamics of controlled variable-speed wind turbines," *IEEE Syst. J.*, vol. 9, no. 2, pp. 639–646, Jun. 2015.
[17] S. Ghosh, S. Kamalasadan, N. Senroy, and J. Enslin, "Doubly fed induction generator (DFIG)-based wind farm control framework for primary frequency and inertial response application," *IEEE Trans. Power Syst.*, vol. 31, no. 3, pp. 1861–1871, May 2016.
[18] M. Toulabi, S. Bahrami, and A. M. Ranjbar, "An input-to-state stability approach to inertial frequency response analysis of doubly-fed induction generator-based wind turbines," *IEEE Trans. Energy Convers.*, vol. 32, no. 4, pp. 1418–1431, Dec. 2017.
[19] L.-R. Chang-Chien, W.-T. Lin, and Y.-C. Yin, "Enhancing frequency response control by DFIGs in the high wind penetrated power systems," *IEEE Trans. Power Syst.*, vol. 26, no. 2, pp. 710–718, May 2011.
[20] A. Zertek, G. Verbic, and M. Pantos, "A novel strategy for variable-speed wind turbines' participation in primary frequency control," *IEEE Trans. Sustain. Energy*, vol. 3, no. 4, pp. 791–799, Oct. 2012.
[21] Z.-S. Zhang, Y.-Z. Sun, J. Lin, and G.-J. Li, "Coordinated frequency regulation by doubly fed induction generator-based wind power plants," *IET Renew. Power Gener.*, vol. 6, no. 1, pp. 38–47, Jan. 2012.
[22] A. S. Ahmadyar and G. Verbi , "Coordinated operation strategy of wind farms for frequency control by exploring wake interaction," *IEEE Trans. Sustain. Energy*, vol. 8, no. 1, pp. 230–238, Jan. 2017.
[23] J. Zhao, X. Lyv, Y. Fu, X. Hu, and F. Li, "Coordinated microgrid frequency regulation based on DFIG variable coefficient using virtual inertia and primary frequency control," *IEEE Trans. Energy Convers.*, vol. 31, no. 3, pp. 833–845, Sep. 2016.
[24] C. Pradhan and C. N. Bhende, "Frequency sensitivity analysis of load damping coefficient in wind farm-integrated power system," *IEEE Trans. Power Syst.*, vol. 32, no. 2, pp. 1016–1029, May 2017.
[25] M. Krpan and I. Kuzle, "Introducing low-order system frequency response modelling of a future power system with high penetration of wind power plants with frequency support capabilities," *IET Renew. Power Gener.*, vol. 12, no. 13, pp. 1453–1461, Oct. 2018.
[26] P. Kundur, *Power System Stability and Control*. New York, NY, USA: McGraw-Hill, 1994, pp. 128–136.
[27] J. H. Chow, *Power System Coherency and Model Reduction*. New York, NY, USA: Springer, 2013, pp. 33–35.
[28] W. Li, P. Chao, X. Liang, J. Ma, D. Xu, and X. Jin, "A practical equivalent method for DFIG wind farms," *IEEE Trans. Sustain. Energy*, vol. 9, no. 2, pp. 610–620, Apr. 2017.
[29] O. Jinxin, D. Yanbo, Z. Di, Y. Rui, Z. Xi, and X. Xiaofu, "Dynamic equivalent model of doubly fed wind farm during electromagnetic transient process," *IET Renew. Power Gener.*, vol. 11, no. 1, pp. 100–106, Jan. 2016.

JIANFENG DAI received the master's degree in electrical engineering from the Shanghai University of Electric Power, Shanghai, China, in 2015. He is currently pursuing the Ph.D. degree with Southeast University, Nanjing, China. His current research interest includes new energy power system stability analysis and control.

YI TANG (M'07–SM'19) received the Ph.D. degree from the Harbin Institute of Technology, Harbin, China, in 2006.

He is currently an Associate Professor with Southeast University, Nanjing, China. His research interests include smart grid, power system security, power system stability analysis, renewable energy systems, and cyber physical systems.

QI WANG (S'13–M'17) received the bachelor's, master's, and Ph.D. degrees in electrical engineering from Southeast University, Nanjing, China, in 2010, 2012, and 2016, respectively.

He is currently a Lecturer with the School of Electrical Engineering, Southeast University. His research interests include power system stability and control, and cyber physical power system.

PING JIANG received the master's degree in electrical engineering from the PLA University of Science and Technology, Nanjing, China, in 1988, and the Ph.D. degree in electrical engineering from Southeast University, Nanjing, China, in 2010.

He is currently a Professor with Southeast University. His research interests include the application of power electronics in power system and renewable energy integration.